

Article

Electrodeposition of Ni-Co Alloys and Their Mechanical Properties by Micro-Vickers Hardness Test

Yiming Jiang ¹, Chun-Yi Chen ², Tso-Fu Mark Chang ^{1,2,*}, Xun Luo ³, Daisuke Yamane ⁴ and Masato Sone ^{1,2}

¹ Department of Material Science and Engineering, Tokyo Institute of Technology, Kanagawa 226-8503, Japan; jiang.y.ag@m.titech.ac.jp (Y.J.); sone.m.aa@m.titech.ac.jp (M.S.)

² Institute of Innovative Research, Tokyo Institute of Technology, 4259 Nagatsuta-cho, Midori-ku, Yokohama, Kanagawa 226-8503, Japan; chen.c.ac@m.titech.ac.jp

³ Key Laboratory of Light Metal Materials Processing Technology of Guizhou Province, Guizhou Institute of Technology, Guiyang 550003, China; cloudlx@163.com

⁴ Department of Mechanical Engineering, Ritsumeikan University, 1-1-1 Noji-Higashi, Kusatsu, Shiga 525-8577, Japan; dyamane@fc.ritsumeik.ac.jp

* Correspondence: chang.m.aa@m.titech.ac.jp; Tel.: +81-45-924-5631

Abstract: Nanocrystalline Ni-Co alloy deposits with grain sizes less than 30 nm were produced by electrodeposition with a direct current in a sulfamate bath. Surfaces of the Ni-Co alloy deposits showed granular morphology. The size of the granular particles and the Co content decreased when a lower current density was applied. Addition of NiBr₂ and a surface brightener (NSF-E) into the bath resulted in the grain refinement effect and an increase of Co content in the deposit. The grain size reached roughly 14 nm and 60 at.% of Co content in Ni-Co alloys electrodeposited with the bath containing the two additives. Ni-Co alloys obtained in this study showed higher microhardnesses than those of pure Ni and Co deposits prepared under the same condition, which revealed the solid solution strengthening effect. With a decrease in the grain size, the microhardness further increased, and this trend followed the Hall–Petch relationship well. The maximum microhardness value of 862.2 Hv was obtained owing to both the grain boundary and solid solution strengthening effects.

Keywords: alloy electrodeposition; Ni-Co alloy; microhardness; grain boundary strengthening; solid solution strengthening



Citation: Jiang, Y.; Chen, C.-Y.; Chang, T.M.; Luo, X.; Yamane, D.; Sone, M. Electrodeposition of Ni-Co Alloys and Their Mechanical Properties by Micro-Vickers Hardness Test. *Electrochem* **2021**, *2*, 1–9. <https://dx.doi.org/10.3390/electrochem2010001>

Received: 2 November 2020

Accepted: 23 December 2020

Published: 24 December 2020

Publisher's Note: MDPI stays neutral with regard to jurisdictional claims in published maps and institutional affiliations.



Copyright: © 2020 by the authors. Licensee MDPI, Basel, Switzerland. This article is an open access article distributed under the terms and conditions of the Creative Commons Attribution (CC BY) license (<https://creativecommons.org/licenses/by/4.0/>).

1. Introduction

Nickel [1], cobalt [2], and their alloys have been investigated as important engineering materials because of their unique properties, such as magnetism, high heat-conductivity, high hardness, and electrocatalytic activity [3]. Much interest is focused on electrodeposition of Ni-Co alloys for application in micro-electrical-mechanical systems (MEMS) devices because of the applicability of the electrodeposition technique in the fabrication of complex three-dimensional micro-scale components, and the excellent electrical, magnetic, and mechanical properties of Ni-Co alloys [4].

On the other hand, in design of a structural component toward electronic devices, mechanical property information of the material is important since the reliability and structure stability of the component are highly dependent on the mechanical properties. For metallic materials, the mechanical properties are closely related to their average grain size according to the grain boundary strengthening mechanism [5]. In most cases, the microhardness is dependent on the average grain size according to the Hall–Petch relationship [6–8]:

$$H_V = H_{V,0} + kd^{-1/2} \quad (1)$$

where H_V is hardness of a polycrystalline metal, $H_{V,0}$ is the friction stress, d is the average grain size, and k is the Hall–Petch coefficient. Based on the Hall–Petch relationship, significant strengthening in metallic materials is obtained by refining the average grain size to

nanoscale (below 100 nm) when compared with coarse-grained counterparts. Some unique properties observed in nanocrystalline materials including enhanced wear resistance and decreased coefficient of friction [9] are in part attributed to the grain size effect caused by the increased interfacial defect volume fraction. Yet, there is a limit for grain boundary strengthening, and further grain refinement would lead to a decrease in the mechanical strength after reaching a critical grain size, which is known as the inverse Hall–Petch relationship. This critical grain size is reported to be below 11 nm for Ni-Co or other Ni alloys (such as Ni-W) [10,11].

Meanwhile, alloying allows utilization of the solid solution strengthening mechanism to realize further enhancement of the mechanical strength [12]. When solute atoms are introduced, local stress fields are formed to initiate interactions with the dislocations, which would impede motions of the dislocations and result an increase in the mechanical strength. Usually, the solid solution strengthening mechanism observed in nanocrystalline alloys is expected to be the same as that in a coarse-grain alloy, and the strengthening effect is known to be mostly depended on the composition in a binary alloy system. In some cases, alloying also enables the realization of finer grain size, which could be refined down to amorphous level [13,14]. For Ni-Co alloys, nickel and cobalt form a solid solution over the whole concentration range due to their close element numbers and similar atom structures, which makes the alloy promising for manipulation of the property toward practical application.

Electrodeposition is widely applied in fabrication of electronic components because of the ease in controlling the morphology, crystal structure, composition, and deposition rate of the electrodeposited materials. For electrodeposition of Ni-Co alloys, the property could be manipulated simply by varying the electrodeposition parameters, such as the current density, bath composition, and temperature [15,16]. For instance, the grain size of electrodeposited materials could be controlled by changing the current density [1,2], pulsed electrodeposition [5,11], the use of ultrasound [17], the use of additive [18], and the introduction of supercritical carbon dioxide emulsions into the electrolyte [19]. An interesting finding in electrodeposition of Ni-Co alloys is that the Co/(Co + Ni) ratio in the electrodeposited alloy is considerably higher than the ratio in the bath since the less noble constituent, which is cobalt here when compare to nickel, is reduced and electrodeposited preferentially [15]. Electrodeposition is particularly effective in refining the average grain size to nanoscale and decoration of non-uniform surfaces [20], which are advantageous in fabrication of electronic components [21]. By integrating electrodeposition technique with lithography process, three dimensional components or metallic micro-patterns can be rapidly fabricated, and the production method has already been applied in the manufacturing process of MEMS devices [22].

There are limited reports on mechanical properties of electrodeposited Ni-Co alloys, and information is required for the design of new electronic devices. Therefore, in this study, the effects of the applied current density and additives on the average grain size, composition, and mechanical properties of electrodeposited Ni-Co alloy deposits are evaluated. The strengthening effects related to the composition and grain size are also discussed.

2. Experiment Methods

2.1. Electrodeposition of Ni-Co Alloy Deposits

The Ni-Co alloy electrodeposition was carried out at 55 °C in a sulfamate bath, and the bath was composed of 300 g/L nickel sulfamate tetrahydrate, 30 g/L cobalt sulfamate tetrahydrate, and 40 g/L boronic acid. Direct current with the current density ranging from 5 to 20 mA/cm² was applied, and the electrodeposition time was adjusted to ensure a charge density of 150 C/cm² for each deposit. More details are listed in Table 1. The film thickness reaches roughly 50 μm when 100% current efficiency is reached. The substrates used in the electrodeposition were 99.96% copper substrates (Kikuya PM Co., Ltd., Tokyo, Japan) measuring 10 × 10 mm². A piece of 99.95% platinum plate (Kikuya PM Co., Ltd., Tokyo, Japan) was used as the counter electrode. The bath was stirred at 220 rpm using

a cross-shape magnetic stirrer. 10 g/L NiBr₂ was added to manipulate properties of the alloy deposits. A surface brightener, 0.5 vol.% NSF-E (Nihon Kagaku Sangyo Co., Ltd., Tokyo, Japan), was used as the brightening additive. A schematic of the electrodeposition is shown in Figure 1.

Table 1. Summary of current density, microhardness, Co content, and grain size of the Ni-Co alloys.

	Current Density (mA/cm ²)	Grain Size (nm)	Co Content (at.%)	Microhardness (Hv)	Sample No.
Without additive	5	21.6	18.19	372.4 ± 12.2	A1
	8	28.9	20.45	433.4 ± 11.3	A2
With NiBr ₂	5	19.2	65.74	295.6 ± 5.9	B1
	10	18.9	62.48	526.0 ± 7.2	B2
	12	29.7	59.82	484.4 ± 15.2	B3
	15	27.8	61.51	490.2 ± 12.0	B4
	18	28.2	55.63	495.6 ± 14.8	B5
	20	20.9	56.67	519.0 ± 15.4	B6
With NiBr ₂ and NSF-E	12	14.1	65.47	760.2 ± 14.2	C1
	15	13.0	66.64	862.2 ± 11.5	C2
	20	14.6	58.48	653.4 ± 15.5	C3
Pure Ni	10	20.6	0	305.8 ± 11.1	Ni
Pure Co	10	27.2	100	402.6 ± 16.9	Co

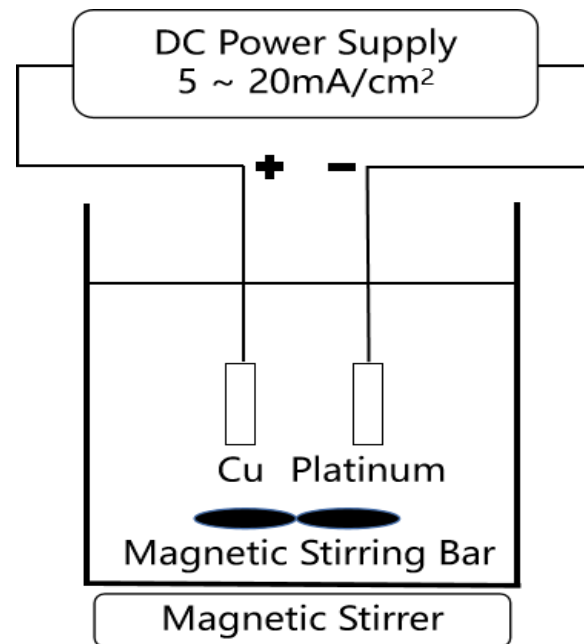


Figure 1. The schematic of the electrodeposition process.

2.2. Characterization of Ni-Co Alloy Deposits

Crystalline structure of the Ni-Co alloy deposits was characterized by X-ray diffraction (XRD, Ultima IV, Rigaku Corp., Tokyo, Japan); the X-ray was generated by a copper target operated at 40 kV and 40 mA. The average grain size (d) was determined using the XRD result in conjunction with the Scherrer equation (see Equation (2)).

$$d = \frac{K\lambda}{\beta \cos \theta} \quad (2)$$

where K is a shape factor; λ is the wave length of X-ray, which is equal to 0.15418 nm; β is the full width at half maximum; and θ is the Bragg angle. Microhardness tests were conducted on a micro hardness tester (HMV-G20S, Shimadzu Corp., Kyoto, Japan) using a load of 0.025 kg (HV 0.025) and a loading time of 15 s. Microhardness results reported were average values of 5 points located in the center and four corners of the alloy deposit. The Ni-Co alloy electrodeposited copper substrates were cut into slices to show cross-section of the deposits. The surface morphology and microstructure of the alloy deposits were investigated using a scanning electron microscope (SEM, SU4300SE Hitachi Co., Ltd., Tokyo, Japan). The composition was analyzed by energy dispersive X-ray spectroscopy system (EDX, EMAX EX-250 Horiba Co., Ltd., Kyoto, Japan) equipped in the SEM.

3. Results and Discussion

3.1. Morphology

Surface morphologies of Ni-Co alloys electrodeposited without addition of the two additives showed granular morphology, and no obvious change was observed when increasing the current density from 5 to 8 mA/cm² as shown in Figure 2. In Figure 3a, the Ni-Co alloy deposit electrodeposited with the bath containing NiBr₂ showed plate-like morphology when the current density was at 5 mA/cm². The edge-rich morphology was also reported in Ni-Co alloy deposits obtained from the bath containing NiSO₄, NiCl₂, CoSO₄, and boric acid [23]. The morphology changed to granular particles as the current density increased to 10 mA/cm², and the average particle size was smaller than that of deposits obtained from the bath with no additive. The change of the morphology from plate-like to granular morphology as the current density increased could be explained by the classic nucleation model [24]. The surface energy of crystalline solids is usually anisotropic, and the applied potential involved in the reduction would be lowered as the current density lowered according to the Butler–Volmer equation. This implies that at a low current density, the Ni-Co alloy would have a preferred growth direction that leads to the edge-rich morphology, and at high current density, the energy involved in reduction of Ni-Co alloy could be high enough to result the granular morphology. As the current density increased to 18 and 20 mA/cm², size of the granular particles enlarged as shown in Figure 3c,d. Morphology of electrodeposited materials is greatly affected by the overpotential. The nucleation is promoted when the overpotential is high, and the particle growth is enhanced at a low overpotential. The overpotential is directly related to the applied current density. When a high applied current density is used, overpotentials of the main reaction (reduction of Ni and Co in this study) would be lowered and resulted a promoted particle growth rate [19]. After addition of the brightener (NSF-E), the surface became smooth as shown in Figure 4.

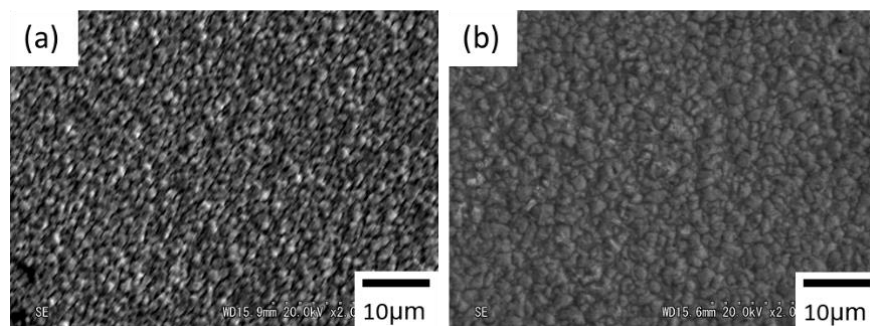


Figure 2. SEM images of Ni-Co alloys electrodeposited without the additives at (a) 5 and (b) 8 mA/cm².

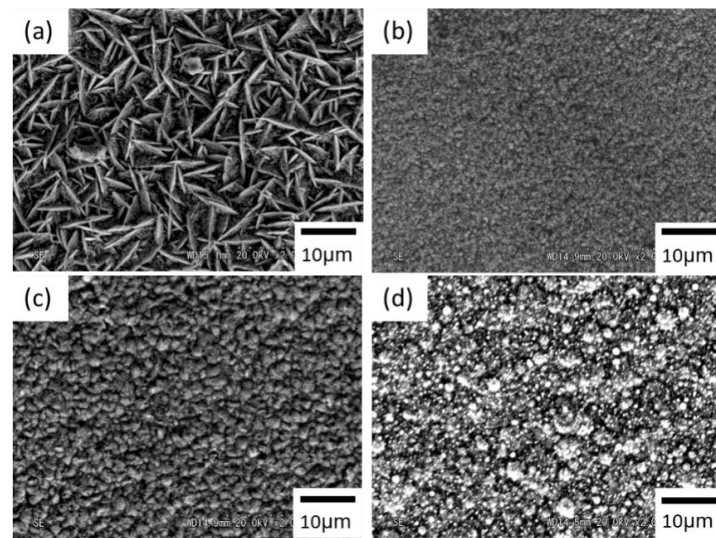


Figure 3. SEM images of Ni-Co alloys electrodeposited with the bath containing NiBr₂ and current density at (a) 5, (b) 10, (c) 18, and (d) 20 mA/cm².

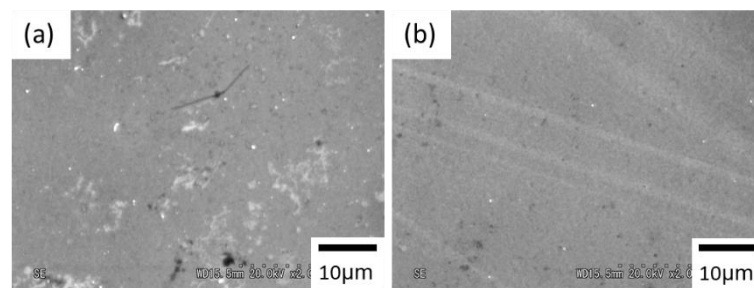


Figure 4. SEM images of Ni-Co alloys electrodeposited with the bath containing both NiBr₂ and NSF-E and current density at (a) 12 and (b) 15 mA/cm².

3.2. Crystal Structure and Grain Size

Ni-Co alloys, pure Ni, and Co deposits obtained in this study all exhibit XRD peaks corresponding to the (111), (200), and (220) planes in the face-centered cubic (FCC) structure as shown in Figure 5. The (111) diffraction peak was the highest for all the Ni-Co alloys. Average grain sizes of these alloys were estimated from the (111) diffraction peaks using the Scherrer equation. The average grain size results were summarized in Table 1.

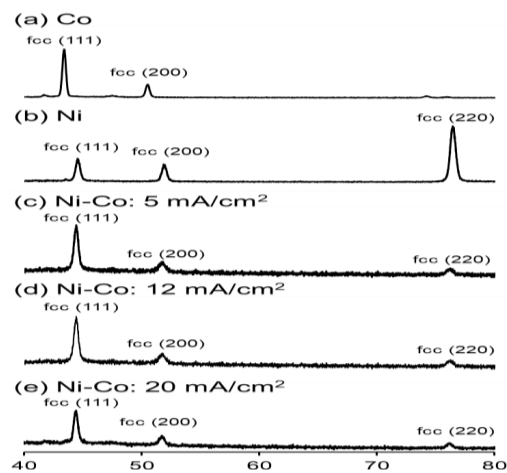


Figure 5. XRD patterns of (a) Co, (b) Ni, and Ni-Co alloy, deposited with the bath containing NiBr₂ and the current density at (c) 5, (d) 12, and (e) 20 mA/cm².

Grain sizes of the Ni-Co alloy deposits obtained from the bath containing no additive (A samples, ●) increased as the current density increased, as shown in Figure 6. Grain refinement was observed after addition of NiBr₂ (B samples, ■) into the bath. For instance, the grain size decreased from 21.6 to 19.2 nm after addition of NiBr₂ when 5 mA/cm² was used. Halides, such as bromide in this study, are reported to act like weak suppressors in electrodeposition, and presence of suppressors in the electrodeposition bath would cause an increase in the overpotential of reduction reactions [25,26], while an increase in the overpotential favors the nucleation that leads to grain refinement of the deposit [27]. For the Ni-Co alloys obtained from NiBr₂-containing bath, no obvious dependency in the grain size was observed when varying the current density from 5 to 20 mA/cm². NSF-E is a surface brightener; surface brighteners are one type of suppressors that cause the grain refinement effect. Hence, further grain refinement was observed in the Ni-Co alloy deposits after addition of the NSF-E.

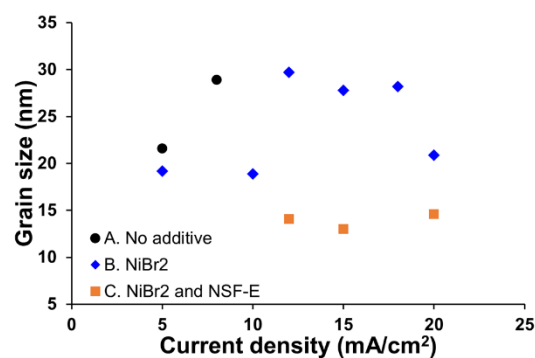


Figure 6. The relationship between the current density and grain size.

3.3. Composition

Co content in the Ni-Co alloy deposits increased as the current density increased when using the bath without the two additives as shown in Figure 7. The standard reduction potential of Co (−0.28 V vs. SHE [28]) is more negative than that of Ni (−0.257 V vs. SHE [28]). Therefore, it is expected to see an increase in the Co content following an increase in the current density. For the Ni-Co alloys electrodeposited with the bath containing NiBr₂, Co content in the alloy deposit significantly increased from roughly 20 to 60 at.% when compared with A samples. This result again revealed that bromide ions in the bath would work like the suppressor to cause an increase in the overpotential that favors reduction of cobalt. Regarding the effect of current density in B samples, the Co content decreased as the current density increased. This tendency was unexpected, but similar results were reported in Ni-Co alloys electrodeposited from a bath containing the suppressors [29]. Ni-Co alloys obtained from the bath containing both NiBr₂ and NSF-E had a higher Co content than those in B samples electrodeposited at the same current density, and the Co content also slightly decreased as the current density increased.

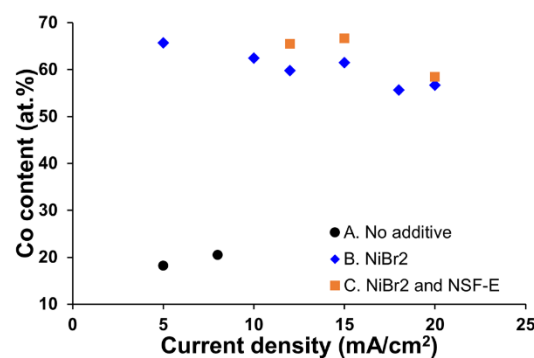


Figure 7. The relationship between the current density and Co content.

3.4. Microhardness

The Hall–Petch plot was prepared to examine relationship between the grain size and the microhardness as shown in Figure 8. Microhardness' of pure Ni and Co deposits prepared in this study were also included in the plot. Generally, strengthening in alloy deposits prepared in this study was observed as the grain size reduced or as the $d^{-1/2}$ increased, which indicates the grain size and microhardness followed the Hall–Petch relationship well [7,8]. B1 sample had a relatively small grain size at 19.2 nm, but the microhardness (295.6 Hv) was the lowest among deposits evaluated in this study. This was a result of the plate-like morphology.

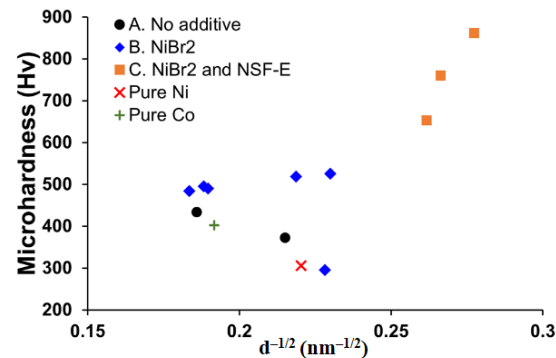


Figure 8. The relationship between the grain size and microhardness.

Figure 9 shows the microhardness of the deposits at different levels of Co content. Excluding microhardness results of A1 (372.4 Hv) and B1 (295.6 Hv), Ni-Co alloys prepared in this study all showed a higher microhardness than those of pure Ni (305.8 Hv) and Co (402.6 Hv), which reveal the strengthening contributed by the solid-solution strengthening mechanism. As shown in Figure 9, the Co content in C samples was at the same level as that in B samples, but C samples showed higher microhardness than those in B samples. This finding indicated a stronger contribution from the grain boundary strengthening on overall mechanical strength of the alloy deposits than that from the solid solution strengthening since the grain sizes of C samples were at roughly 14 nm and the grain sizes of B samples were at 20–30 nm level. The highest microhardness obtained in this study was 862.2 Hv from the Ni-Co alloy (sample C2) composed of the finest grain size at 13.0 nm.

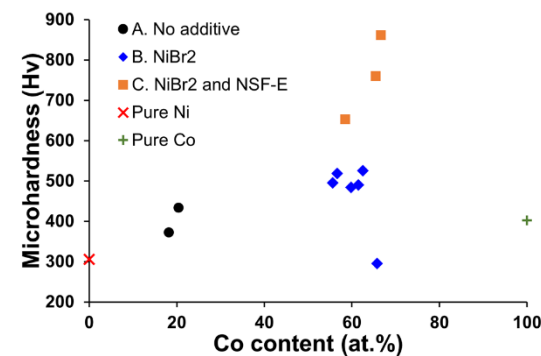


Figure 9. The relationship between the Co content and microhardness.

4. Conclusions

Ni-Co alloy deposits were electrodeposited in a sulfamate bath. The Ni-Co alloy deposits showed granular morphology except for the one electrodeposited with the bath containing NiBr₂ and the current density at 5 mA/cm², whose the surface showed plate-like morphology. Refinement in the average grain size was observed after introduction of NiBr₂ and a surface brightener (NSF-E) into the bath. The Co content increased from ca. 20 to 60 at.% after addition of NiBr₂ and NSF-E into the bath. The microhardness was

confirmed to be affected by both the grain size and the Co content, and the dependency was higher on the grain size. The microhardness reached 862.2 Hv in a Ni-Co alloy deposit having 13.0 nm grain size and 66.64 at.% Co content.

Author Contributions: Conceptualization, Y.J. and T.-F.M.C.; Methodology, Y.J.; Validation, C.-Y.C., X.L. and D.Y.; Formal analysis, Y.J.; Investigation, Y.J. and T.-F.M.C.; Resources, T.-F.M.C.; Data curation, Y.J.; Writing—original draft preparation, Y.J.; Writing—review and editing, C.-Y.C. and T.-F.M.C.; Visualization, Y.J.; Supervision, T.-F.M.C. and M.S.; Project administration, M.S.; Funding acquisition, T.-F.M.C. and M.S. All authors have read and agreed to the published version of the manuscript.

Funding: This research was funded by the New Energy and Industrial Technology Development Organization (NEDO).

Institutional Review Board Statement: Not applicable.

Informed Consent Statement: Not applicable.

Data Availability Statement: The data presented in this study are available on request from the corresponding author.

Conflicts of Interest: On behalf of all of the co-authors, the corresponding author states that there is no conflict of interest.

References

1. Yamamoto, T.; Igawa, K.; Tang, H.C.; Chen, C.Y.; Chang, T.F.M.; Nagoshi, T.; Kudo, O.; Maeda, R.; Sone, M. Effects of current density on mechanical properties of electroplated nickel with high speed sulfamate bath. *Microelectron. Eng.* **2019**, *213*, 18–23. [[CrossRef](#)]
2. Luo, X.; Chen, C.Y.; Chang, T.F.M.; Hosoda, H.; Sone, M. Crystal growth of cobalt film fabricated by electrodeposition with dense carbon dioxide. *J. Electrochem. Soc.* **2015**, *162*, D423–D426. [[CrossRef](#)]
3. Cole, K.M.; Kirk, D.W.; Thorpe, S.J. In Situ Raman Study of Amorphous and Crystalline Ni-Co Alloys for the Alkaline Oxygen Evolution Reaction. *J. Electrochem. Soc.* **2018**, *165*, J3122–J3129. [[CrossRef](#)]
4. Duch, M.; Esteve, J.; Gómez, E.; Pérez-Castillejos, R.; Vallés, E. Electrodeposited Co-Ni alloys for MEMS. *J. Micromech. Microeng.* **2002**, *12*, 400–405. [[CrossRef](#)]
5. Chen, C.Y.; Yoshida, M.; Nagoshi, T.; Chang, T.F.M.; Yamane, D.; Machida, K.; Masu, K.; Sone, M. Pulse electroplating of ultra-fine grained Au films with high compressive strength. *Electrochem. Commun.* **2016**, *67*, 51–54. [[CrossRef](#)]
6. Hughes, G.D.; Smith, S.D.; Pande, C.S.; Johnson, H.R.; Armstrong, R.W. Hall-petch strengthening for the microhardness of twelve nanometer grain diameter electrodeposited nickel. *Scr. Metall.* **1986**, *20*, 93–97. [[CrossRef](#)]
7. Hall, E.O. The Deformation and Ageing of Mild Steel: III Discussion of Results. *Proc. Phys. Soc. Lond. Sect. B* **1951**, *64*, 747–753. [[CrossRef](#)]
8. Petch, N.J. The orientation relationships between cementite and α -iron. *Acta Cryst.* **1953**, *6*, 96. [[CrossRef](#)]
9. Sriraman, K.R.; Raman, S.G.S. Synthesis and evaluation of hardness and sliding wear resistance of electrodeposited nanocrystalline Ni-W alloys. *Mater. Sci. Eng. A* **2006**, *418*, 303–311. [[CrossRef](#)]
10. Giga, A.; Kimoto, Y.; Takigawa, Y.; Higashi, K. Demonstration of an inverse Hall-Petch relationship in electrodeposited nanocrystalline Ni-W alloys through tensile testing. *Scr. Mater.* **2006**, *55*, 143–146. [[CrossRef](#)]
11. Li, Y.; Jiang, H.; Huang, H. Effects of peak current density on the mechanical properties of nanocrystalline Ni-Co alloys produced by pulse electrodeposition. *Appl. Surf. Sci.* **2008**, *254*, 6865–6869. [[CrossRef](#)]
12. Tang, H.; Chang, T.F.M.; Chai, Y.W.; Chen, C.Y.; Nagoshi, T.; Yamane, D.; Ito, H.; Machida, K.; Masu, K.; Sone, M. Nanoscale Hierarchical Structure of Twins in Nanograins Embedded with Twins and the Strengthening Effect. *J. Electrochem. Soc.* **2018**, *165*, D58–D63. [[CrossRef](#)]
13. Schuh, C.A.; Nieh, T.G.; Iwasaki, H. The effect of solid solution W additions on the mechanical properties of nanocrystalline Ni. *Acta Mater.* **2003**, *51*, 431–443. [[CrossRef](#)]
14. Han, B.Q.; Lavernia, E.J. Deformation Mechanisms of Nanostructured Al Alloys. *Adv. Eng. Mater.* **2005**, *7*, 457–465. [[CrossRef](#)]
15. Bai, A.; Hu, C.C. Effects of electroplating variables on the composition and morphology of nickel-cobalt deposits plated through means of cyclic voltammetry. *Electrochim. Acta* **2002**, *47*, 3447–3456. [[CrossRef](#)]
16. Hu, C.C.; Wang, C.K. Effects of composition and reflowing on the corrosion behavior of Sn-Zn deposits in brine media. *Electrochim. Acta* **2006**, *51*, 4125–4134. [[CrossRef](#)]
17. Tudela, I.; Zhang, Y.; Pal, M.; Kerr, I.; Cobley, A.J. Ultrasound-assisted electrodeposition of composite coatings with particles. *Surf. Coat. Technol.* **2014**, *259*, 363–373. [[CrossRef](#)]
18. Kolonits, T.; Czigány, Z.; Péter, L.; Bakonyi, I.; Gubicza, J. Influence of bath additives on the thermal stability of the nanostructure and hardness of Ni films processed by electrodeposition. *Coatings* **2019**, *9*, 644. [[CrossRef](#)]
19. Chang, T.F.M.; Sone, M.; Shibata, A.; Ishiyama, C.; Higo, Y. Bright nickel film deposited by supercritical carbon dioxide emulsion using additive-free Watts bath. *Electrochim. Acta* **2010**, *55*, 6469–6475. [[CrossRef](#)]

20. Park, D.-Y.; Park, K.S.; Ko, J.M.; Cho, D.-H.; Lim, S.H.; Kim, W.Y.; Yoo, B.Y.; Myung, N.V. Electrodeposited Ni_{1-x}Co_x Nanocrystalline Thin Films: Structure–Property Relationships. *J. Electrochem. Soc.* **2006**, *153*, C814–C821. [[CrossRef](#)]
21. Myung, N.V.; Park, D.Y.; Yoo, B.Y.; Sumodjo, P.T.A. Development of electroplated magnetic materials for MEMS. *J. Magn. Mater.* **2003**, *265*, 189–198. [[CrossRef](#)]
22. Nitta, K.; Chang, T.F.M.; Tang, H.; Chen, C.Y.; Iida, S.; Yamane, D.; Machida, K.; Ito, H.; Masu, K.; Sone, M. Alloy electroplating and Young's modulus characterization of AuCu alloy microcantilevers. *J. Electrochem. Soc.* **2020**, *167*, 082503. [[CrossRef](#)]
23. Shi, L.; Sun, C.; Liu, W. Electrodeposited nickel–cobalt composite coating containing MoS₂. *Appl. Surf. Sci.* **2008**, *254*, 6880–6885. [[CrossRef](#)]
24. Sau, T.K.; Rogach, A.L. Nonspherical noble metal nanoparticles: Colloid-chemical synthesis and morphology control. *Adv. Mater.* **2010**, *22*, 1781–1804. [[CrossRef](#)]
25. Tsuru, Y.; Nomura, M.; Foulkes, F.R. Effects of chloride, bromide and iodide ions on internal stress in films deposited during high speed nickel electroplating from a nickel sulfamate bath. *J. Appl. Electrochem.* **2000**, *30*, 231–238. [[CrossRef](#)]
26. Huynh, T.M.T.; Wess, F.; Hai, N.T.M.; Reckien, W.; Bredow, T.; Fluegel, A.; Arnold, M.; Mayer, D.; Keller, H.; Broekmann, P. On the role of halides and thiols in additive-assisted copper electroplating. *Electrochim. Acta* **2013**, *89*, 537–548. [[CrossRef](#)]
27. Moti, E.; Shariat, M.H.; Bahrololoom, M.E. Influence of cathodic overpotential on grain size in nanocrystalline nickel deposition on rotating cylinder electrodes. *J Appl. Electrochem.* **2008**, *38*, 605–612. [[CrossRef](#)]
28. Vanýsek, P. Electrochemical series. In *Handbook of Chemistry and Physics*, 93th ed.; Haynes, W.M., Ed.; CRC Press: New York, NY, USA, 2012; pp. 5–88.
29. Burzyńska, L.; Rudnik, E. The influence of electrolysis parameters on the composition and morphology of Co–Ni alloys. *Hydrometallurgy* **2000**, *54*, 133–149. [[CrossRef](#)]